Adiabatic theory of Wannier threshold laws and ionization cross sections

J. H. Macek and S. Yu. Ovchinnikov*
Department of Physics and Astronomy, University of Tennessee, Knoxville, Tennessee 37996-1501
and Oak Ridge National Laboratory, P. O. Box 2009, Oak Ridge, Tennessee 37831
(Received 31 January 1994)

Adiabatic energy eigenvalues of H_2^+ are computed for complex values of the internuclear distance R. The infinite number of bound-state eigenenergies are represented by a function $\epsilon(R)$ that is single valued on a multisheeted Riemann surface. A region is found where $\epsilon(R)$ and the corresponding eigenfunctions exhibit harmonic-oscillator structure characteristic of electron motion on a potential saddle. The Schrödinger equation is solved in the adiabatic approximation along a path in the complex R plane to compute ionization cross sections. The cross section thus obtained joins the Wannier threshold region with the keV energy region, but the exponent near the ionization threshold disagrees with well-accepted values. Accepted values are obtained when a lowest-order diabatic correction is employed, indicating that adiabatic approximations do not give the correct zero velocity limit for ionization cross sections. Semiclassical eigenvalues for general top-of-barrier motion are given and the theory is applied to the ionization of atomic hydrogen by electron impact. The theory with a first diabatic correction gives the Wannier threshold law even for this case.

PACS number(s): 34.80.Dp

I. INTRODUCTION

The collective motion of charged particles is fundamental to atomic physics. Many insights concerning this motion have emerged, but the critical importance of motion near the saddle point of the potential energy of two-electron atoms has been particularly significant [1–20]. The Wannier threshold law for ionization of neutral atoms by electron impact is one of the most striking consequences of saddle point motion. Threshold law theories, originally used to describe two electrons in the field of a proton or α particle, have been developed for three fragments of arbitrary masses and charges [4,7]. Typically, threshold laws apply only when wavelengths of the Schrödinger waves for all particle pairs are greater than, or of the order of, the dimension of the initial bound state wave function; thus, the extent of the energy region where the laws apply is of the order of $1/m_P$ smaller for proton impact ionization of atom hydrogen than for electron impact. Here, m_P is the proton mass in atomic units. In contradiction to this are calculations of ionization cross sections in proton-hydrogen collisions which suggest that motion on the potential saddle, also called top-of-barrier motion, represents an important channel for proton energies as high as 25 keV [19]. In this extended energy region, the cross section varies with energy E as $\exp[-C\sqrt{m_P/2E}]$, where C is a constant rather than as $(E - E_{\rm thresh})^{\zeta}$, where $E_{\rm thresh}$ is the threshold energy and ζ is the Wannier exponent. Since the theory used to establish power laws is not readily applied at keV energies, the common origin of the two expressions above for the cross sections is not readily apparent even though the top-of-barrier mechanism underlies both of them. It is desirable to devise a theoretical framework that encompasses both results. This report describes such a framework. In order to emphasize the simplicity of the results, only the total cross section is computed. Other aspects such as energy and angular distributions of charged fragments can also be obtained, but require more elaborate computations than those needed for total ionization cross sections.

A wave function, $\Psi(R,x)$, corresponding to motion near the top of the barrier is central to our computations. For this purpose a reaction coordinate R, which measures the overall size of the three-particle system, is selected. The remaining coordinates of the multiparticle system are denoted generically by the set $x = \{x_1, x_2, ..., x_N\}$. The exact specification of these coordinates depends upon the particular physical context. It is important to note, however, that these coordinates x are dimensionless. When R represents the hyperradius, then x denotes a set of hyperangles. Alternatively, when R denotes the distance between two nuclei, as is customary in ion-atom collisions, the set x denotes components of the scaled electron coordinate $\mathbf{r}/R$. Solov'ev and Vinitsky [21] demonstrate that this prescription is appropriate for adiabatic representations of atomic dynamics employing transient molecular eigenstates. Adiabatic descriptions of motion orthogonal to R identify a sequence of broad avoided crossings between eigenvalue curves that lead to excitation and ionization [15]. Because these crossings are not localized at particular values of R, integration of the Schrödinger equation involves solving a large number of coupled channel equations. In the work reported here we emphasize that the solution of any differential equation to connect a function at $R = R_0$ to a solution at $R \to \infty$ may proceed along any path in the complex R plane. In this extended domain it is possible to find a path

*Permanent address: Ioffe Physical-Technical Institute, St. Petersburg, Russia.

along which the crossings representing top-of-barrier motion are well localized. Thus, it is possible to identify a diabatic wave function $\varphi_T(R,x)$ for motion in all coordinates orthogonal to R. The Schrödinger equation is then integrated approximately along this particular path to obtain the probability for ionization as a function of total energy E. In order to connect this simple procedure with the general theory of wave function propagation, we rewrite the multiparticle Schrödinger equation in a form amenable to semiclassical treatments for arbitrary complex R in Sec. II. Section III describes the diabatic energy eigenvalue $\epsilon_T(R)$ for top-of-barrier motion and identifies a path in the complex R plane along which a diabatic semiclassical approximation applies. Expressions for ionization cross sections are given and discussed in Sec. IV. Concluding remarks are given in Sec. V.

II. WAVE-FUNCTION PROPAGATION IN THE COMPLEX R-PLANE

Propagation of wave functions, $\psi(R,x)$, that satisfy second-order differential equations in R usually employ Green functions. Alternatively, when $\psi(R,x)$ satisfies a first-order differential equation in R, a variant of Feynman's propagator may be used. The latter representation of wave-function propagation is more suitable for our purposes [22]. To that end we rewrite the generic second-order Schrödinger equation

$$\left[-\frac{1}{2M}\frac{\partial^2}{\partial R^2}+\mathcal{H}(R,x)-E\right]\psi=0 \tag{2.1}$$

as two-coupled first-order equations by introducing the operator $\hat{k}(R)$

$$\hat{k}^2(R)=2M[E-\mathcal{H}(R,x)]\,, \tag{2.2}$$

and the two component wave function $\hat{\psi}$

$$\hat{\psi}=\begin{pmatrix}\psi\\ \frac{\partial\psi}{\partial R}\end{pmatrix}\,, \tag{2.3}$$

so that Eq. (2.1) becomes

$$\frac{\partial\hat{\psi}}{\partial R}+\begin{pmatrix}0 & -1\\ \hat{k}^2(R) & 0\end{pmatrix}\hat{\psi}=0\,. \tag{2.4}$$

Since Eq. (2.4) is first order in R, Feynman's propagator could be introduced at this stage; however, the two components of $\hat{\psi}$ in Eq. (2.4) are strongly coupled, thus, it is not convenient for writing approximate solutions. Rather, we introduce an "adiabatic" representation by defining

$$\hat{\psi}=U(R)\hat{\Psi}\,, \tag{2.5}$$

where

$$U(R)=\begin{pmatrix}1 & -1\\ i\hat{k}(R) & i\hat{k}(R)\end{pmatrix}\,. \tag{2.6}$$

Substituting Eq. (2.5) into (2.4) and multiplying by $iU^{-1}(R)$ gives

$$i\frac{\partial\hat{\Psi}}{\partial R}-\hat{k}(R)\begin{pmatrix}1 & 0\\ 0 & -1\end{pmatrix}\hat{\Psi}+\frac{1}{2}\hat{k}^{-1}(R)\hat{k}'(R)\begin{pmatrix}1 & 1\\ 1 & 1\end{pmatrix}\hat{\Psi}=0\,, \tag{2.7}$$

where the prime on $\hat{k}(R)$ denotes the derivative with respect to R.

This representation is equivalent to Eq. (2.1) but differs from it in that, like Eq. (2.4), it is first order in R. In addition, it is written so that wave propagation is represented as two equations with outgoing waves coupled to incoming waves. Corresponding to Eq. (2.7) one has, exactly,

$$\hat{\Psi}(R,x)=\int K(R,x;R',x')\hat{\Psi}(R',x')dx'\,, \tag{2.8}$$

where $K(R,x;R',x')$ is the propagator corresponding to the two-component Schrödinger equation (2.7).

It must be emphasized that Eq. (2.8) is exact and applies for nearly arbitrary complex R and R'. In order to employ Eq. (2.8), approximate representations of the propagator are needed. Here, it is possible to take advantage of the flexibility implied by the use of complex coordinates to find a path in the complex R plane along which standard approximate representations are valid. Specifically, a path along which the adiabatic representation

$$\hat{\Psi}(R,x)\approx\varphi_T(R;x)\hat{F}(R) \tag{2.9}$$

holds is sought. The two-component function $\hat{F}(R)$ is determined variationally. The adiabatic eigenfunctions, $\varphi_T(R;x)$, and eigenvalues, $\epsilon_T(R)$, satisfy the Schrödinger equation

$$\mathcal{H}(R,x)\varphi_T(R;x)=\epsilon_T(R)\varphi_T(R;x)\,. \tag{2.10}$$

The wave vector, $k_T(R)$, is then given by

$$k_T(R)=\sqrt{2M[E-\epsilon_T(R)]}, \tag{2.11}$$

where Eq. (2.9) implies the approximation

$$\hat{k}'(R)\varphi_T(R;x)\approx\frac{dk_T(R)}{dR}\varphi_T(R;x)\,. \tag{2.12}$$

Equation (2.9) is the appropriate adiabatic representation when R represents the hyperradius. Our applications employ the more conventional coordinate systems where R represents the distance between like charges. In this case Ref. [13] shows that Eq. (2.9) must also incorporate the factor $\exp[ix^2Rk_T(R)/M]$. Our formulas, therefore, include this factor, recognizing that it is not present in the hyperspherical representation originally employed for the fragmentation of atoms into two electrons and a positive ion.

Coupling between incoming and outgoing waves is also

neglected. Then, we have that

$$\Psi(R,x) = \exp[ix^2 R k_T(R)/M]\varphi_T(R;x)k_T(R)^{-1/2} \times \exp\left[i\int_{R_0}^{R} k_T(R')dR'\right] , \quad (2.13)$$

where the integral from R_0 to R is taken along some path in the complex R plane along which the adiabatic and semiclassical approximations implicit in Eq. (2.13) are valid. The coordinate R is generally complex, thus, the approximate wave function may not be valid at the desired final value of $R = R_f$. For present purposes, this is of no concern since $R_f \to \infty$ and $1/R_f = 0$, so that it is not necessary to return to the real axis to use the approximate wave function.

The top-of-barrier function for finite R_f includes components that represent excitation of states of high n as well as ionization, but as $R_f \to \infty$, then $\varphi_T(R;x)$ corresponds to free fragments, and the ionization probability for a given E is given by the standard formula [23]

$$P(E) = \exp\left[-2\,\mathrm{Im}\int_{R_0}^{R_f} k_T(R')dR'\right] . \quad (2.14)$$

It is only necessary to find $\epsilon_T(R)$ and the appropriate path in the complex plane to evaluate the ionization probability.

III. TOP-OF-BARRIER EIGENSTATES

A. Eigenstates of H_2^+ for complex R

Consider systems of three charged particles where R represents the distance between two particles of like charge. Then the adiabatic eigenstates are just the conventional H_2^+ molecular eigenstates. The eigenvalues $\epsilon(R)$ have been computed using the program of Ovchinnikov and Solov'ev [10]. Figure 1 shows a three-dimensional plot of the real part of $\epsilon(R)$ vs $\mathrm{Re}\sqrt{R}$ and $\mathrm{Im}\sqrt{R}$. Note that $\epsilon(R)$ is a single-valued function on a Riemann surface with an infinite number of sheets [24]. On the real axis $\epsilon(R)$ equals a molecular energy eigenvalue; just which of the infinite number of eigenvalues it equals is determined by the particular sheet of the Riemann surface. The different sheets are joined at branch points at complex values of R. In the adiabatic approximation, reaction probabilities are given by Eq. (2.14) with a path in the complex plane chosen to connect the eigenvalue, $\epsilon_i(R)$, on the real axis corresponding to the initial state, i, with the eigenvalue, $\epsilon_f(R)$, corresponding to the final state, f. In the present case i represents an initial $1s\sigma$ united atom eigenstate near $R \approx 0$ but the final state corresponds to an ionized electron continuum state as $R \to \infty$. The adiabatic approximation for the propagator is only valid for finite values of R and a more suitable approximation must be employed as $R \to \infty$. In the present work, the free particle propagator is employed to propagate the top-of-barrier function from finite, but large, R to infinite R. Since only total cross sections are computed, this joining need not be actually carried out explicitly, rather to first approximation the upper limit in Eq. (2.14) is set to infinity.

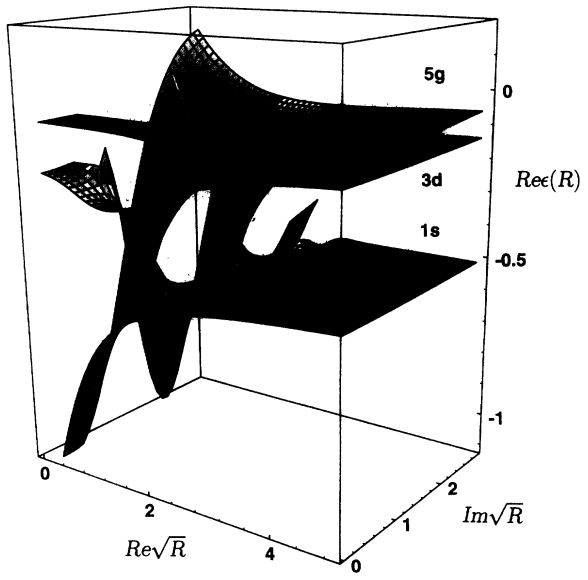

FIG. 1. Plot of the real part of the energy function $\epsilon(R)$ vs complex R. The plot represents a Riemann surface on which $\epsilon(R)$ is a single-valued function. The values along the real axis are the energy eigenvalues $\epsilon_n(R)$ of H_2^+.

The key step is to find an appropriate path in the complex R plane. To find such a path, we follow Ref. [15] and plot $n(R) = 1/\sqrt{-\epsilon(R)}$ vs $\sqrt{R}$ in Fig. 2. Figure 2(a) shows a view with the values on the real axis foremost. The branch points connecting the $1s$-$3d$-$5g$ sheets are clearly visible. These branch points have been previously identified as the T-series branch points. The avoided crossing of the energy curves are visible for real R but merge with a remarkably flat and structureless surface for values $\mathrm{Im}R$ greater than the values corresponding to the branch points. The view in Fig. 2(b) shows this structureless region from the "back" side. It is apparent that an appropriate path in the complex R plane goes from a value of R_0 of the order of one atomic unit on the real axis where the intial state is a $1s\sigma$ state, along a path which runs parallel to the $\mathrm{Im}\sqrt{R}$ axis and then to infinite R on the flat sloping surface. While it is possible to use the numerical eigenvalue $\epsilon(R)$, the simplicity of the surface corresponding to top-of-barrier motion indicates that an analytic treatment to extract the essential features is more informative. Such a treatment is given in the next section.

B. Top-of-barrier eigenvalues and eigenstates

The Hamiltonian $\mathcal{H}(R;x)$ is quite general. As demonstrated originally by Wannier and later by several workers [1–3,6,17,18], motion on the top of potential surfaces along coordinates where the surface has, locally, the shape of an inverted oscillator is critical for atomic

reactions. The classically unstable motion is modeled by the Hamiltonian

$$\mathcal{H}(R;x) = -\frac{1}{2m}\frac{\partial^2}{\partial x^2} + V(R;x)\,, \tag{3.1}$$

where $V(R;x)$ is shown schematically in Fig. 3 at some value of the parameter R. Note that the mass m includes a factor of R^2 in accord with Eq. (11) of Ref. [19] and with

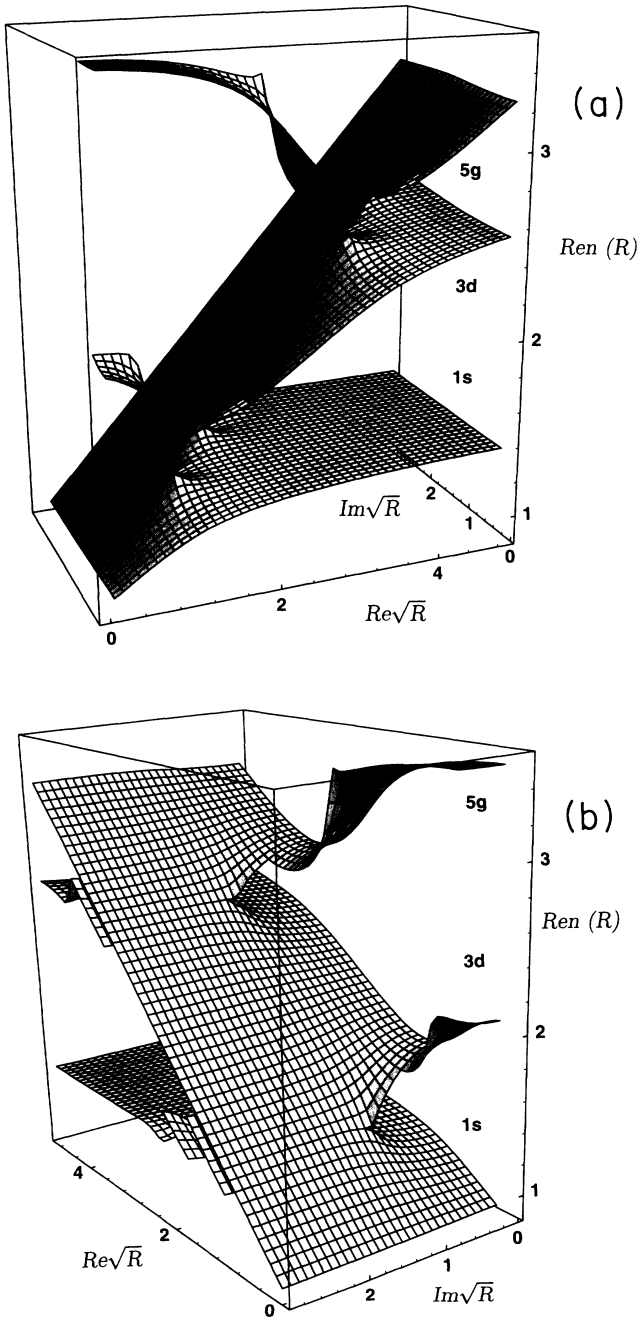

FIG. 2. Plot of $1/\sqrt{\epsilon(R)}$ vs $\sqrt{R}$. (a) "Front" view of the surface with the real axis foremost. (b) "Back" view of the surface showing a sloping flat region to the left of an infinite series of branch points. The first two branch points of this series where the $1s\sigma$-$3d\sigma$-$5g\sigma$ sheets join are exposed in the latter view.

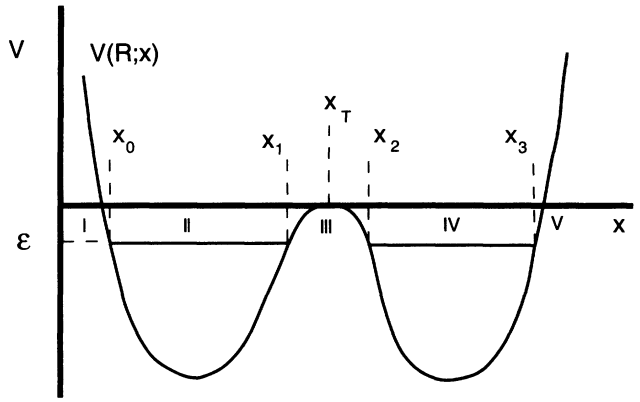

FIG. 3. Schematic plot of a potential $V(R;x)$ with two valley regions and a top-of-barrier region. For a given energy ϵ five coordinate regions are identified. Turning points x_i, $i = 0, 1, 2, 3$ and a top of barrier position x_T are shown.

the hyperspherical representation of Macek [25]. Also x is measured from the center of mass of the two particles of like charge. This origin need not coincide with the center of charge; however, in the remainder of this report only systems for which the center of mass and the center of charge coincide are considered.

We now solve the equation

$$\mathcal{H}(R;x)\varphi(R;x) = \epsilon\varphi(R;x) \tag{3.2}$$

using the semiclassical comparison equation approximation since this approximation is sufficiently accurate for Coulomb potentials. To that end five regions are identified in Fig. 3. In the following the dependence of quantities on R is suppressed for notational simplicity.

The semiclassical wave functions in regions I and II are

$$\psi_{\rm I} = q(x)^{-1/2}\exp\left[-\int_x^{x_0} -q(x')dx'\right]\,, \tag{3.3}$$

$$\psi_{\rm II} = 2q(x)^{-1/2}\cos\left[\int_{x_0}^{x} q(x')dx' - \pi/4\right]$$
$$= 2q(x)^{-1/2}\cos\left[\phi_2 - \int_{-x_1}^{-x} q(x')dx' - \pi/4\right]\,, \tag{3.4}$$

where we have introduced

$$\phi_2 = \int_{x_0}^{x_1} q(x')dx'. \tag{3.5}$$

The function $q(x)$ is defined as

$$q(x) = \sqrt{2m[\epsilon - V(R;x)]}\,, \tag{3.6}$$

where the branch cut is taken such that $\mathrm{Re}\sqrt{2m[V(R;x) - \epsilon - i\eta]} > 0$ for $\eta > 0$. The origin is chosen at the top-of-barrier position, $x_T = 0$, so that $-x_1$ and $-x$ are positive. The choice of origin, $x_T = 0$, is consistent with the adiabatic representation of Eq. (2.13) when the center of mass of the two particles of like charge coincides with their center of charge. This condition is assumed in the following.

The semiclassical function, $\psi_{\rm II}(x)$, is joined with an appropriate solution in the top-of-barrier region III. In this region the potential is approximately an inverted harmonic oscillator for which solutions of the Schrödinger equation are parabolic cylinder functions $E(a,[-4mV''(R;x_T)]^{1/4}x)$, with

$$a=\frac{1}{\pi}\int_{x_1}^{x_2}q(x')dx\ , \tag{3.7}$$

according to the comparison equation method [26]. For $\epsilon < V(R;x), x_1 = x_2^*$ are the complex zeros of $q(x)$. To match solutions in regions II and III note that $E(a,[-4mV''(R;x_T)]^{1/4}x)$ may be written

$$E(a,[-4mV''(R;x_T)]^{1/4}x)=[q(x)]^{-1/2}\exp[iu(x)]\ , \tag{3.8}$$

where

$$u(x)\to\int_{2\sqrt{a}}^{x}q(x')dx'+\pi/4+\phi_0 \tag{3.9}$$

as $x\to\infty$ and

$$\phi_0=\frac{1}{2}\arg\Gamma\left(\frac{1}{2}+ia\right)+\frac{a}{2}(1-\ln|a|)\ ; \tag{3.10}$$

so that Eq. (3.4) becomes

$$\begin{aligned}\psi_{\rm II}&=2[q(x)]^{-1/2}\cos[\phi_2+\phi_0-u(-x)]\\&=[q(x)]^{-1/2}\exp[-iu(-x)]\\&\quad\times\exp[i(\phi_2+\phi_0)]+\text{c.c.}\ ,\end{aligned} \tag{3.11}$$

where c.c. denotes complex conjugate.

Recalling Eq. (3.8), we easily write the solution in region III as

$$\begin{aligned}\psi_{\rm III}&=\exp[i(\phi_2+\phi_0)]\\&\quad\times E^*(a,-[-4mV''(R;x_T)]^{1/4}x)+\text{c.c.}\end{aligned} \tag{3.12}$$

$$\begin{aligned}&=\sqrt{1+e^{2\pi a}}\{-i[e^{i(\phi_2+\phi_0)}+Ae^{-i(\phi_2+\phi_0)}]\\&\quad\times E(a,[-4mV''(R;x_T)]^{1/4}x)+\text{c.c.}\},\end{aligned} \tag{3.13}$$

where we have used Eq. (19.18.3) of Abramowitz and Stegun [27] in the second line and have defined

$$A=1/\sqrt{1+e^{-2\pi a}}. \tag{3.14}$$

As before, the wave function in region IV, where x is positive is

$$\begin{aligned}\psi_{\rm IV}(x)&=\sqrt{1+e^{2\pi a}}[q(x)]^{-1/2}\{[1+Ae^{-2i(\phi_2+\phi_0)}]\\&\quad\times e^{i[\phi_2+\phi_4(x)+2\phi_0-\pi/4]}+\text{c.c.}\},\end{aligned} \tag{3.15}$$

where

$$\phi_4(x)=\int_{x_2}^{x}q(x')dx'\ , \tag{3.16}$$

and Eq. (3.8) has been used.

This function is joined with a WKB solution in region V to determine the quantization conditions. These conditions are derived in detail in Appendix A. The quantization conditions are given by Eqs. (A5) and (A6) which read:

$$\phi_4+\phi_2+2\phi_0\pm\arccos[A\cos(\phi_4-\phi_2)]=\pi(2n+1)\ , \tag{3.17}$$

where $\phi_4=\phi_4(x_3)$.

For potentials which are symmetric about the top of the barrier, $\phi_4=\phi_2$, it is shown in Appendix A that the quantization condition Eq. (3.17) can be written as Eq. (A19), namely,

$$\begin{aligned}\phi_4+\arg\Gamma\left(\frac{1}{2}\mp\frac{1}{4}+i\frac{a}{2}\right)+\frac{a}{2}\left(1-\ln\frac{|a|}{2}\right)\\=\pi\left(n+\frac{1}{2}\mp\frac{1}{8}\right)\ .\end{aligned} \tag{3.18}$$

Here " $-$ " refer to g states and " $+$ " to u states.

Equation (3.17) determines the adiabatic energy levels for all eigenstates of $\mathcal{H}(R,x)$. For energies well above the top of the barrier the parameter a is large and negative so that $A\to 0$, $\phi_0\to 0$ and Eq. (3.17) becomes just the usual united atom semiclassical quantization condition

$$\phi_4+\phi_2=\int_{x_0}^{x_3}q(x)dx=(n_{\rm ua}+1/2)\pi\ , \tag{3.19}$$

where n_{ua} is the united atom quantum number corresponding to the x coordinate. For the $H_2{}^+$ systems this equation gives the united atom adiabatic energy eigenvalues. Conversely, for energies well below the top of the barrier, a is large and positive so $A\to 1$, $\phi_0\to 0$ and Eq. (3.17) becomes just the semiclassical quantization condition for a particle in one of the potential wells on either side of the barrier

$$\phi_2=\int_{x_0}^{x_1}q(x)dx=(n_1+1/2)\pi \tag{3.20}$$

or

$$\phi_4=\int_{x_2}^{x_3}q(x)dx=(n_2+1/2)\pi. \tag{3.21}$$

For the $H_2{}^+$ system this equation gives the separated atom adiabatic energy eigenvalues. As pointed out in Ref. [15], it is precisely the adiabatic energy eigenvalues near the top of the barrier that exhibit a series of broad avoided crossings in the region of R where united atom levels join with separated atom levels. Accordingly, we seek an approximate version of Eq. (3.17) valid in the avoided crossing region by expanding $\phi_2(R)$, $\phi_4(R)$, and $a(R)$ in Eq. (3.7) about the top-of-barrier energy $V(R;x_T)$. Here the dependence of these parameters upon R is denoted explicitly. In lowest order $a(R)$ becomes

$$a(R) = \sqrt{\frac{m}{-V''(R;x_T)}}[V(R;x_T) - \epsilon]. \quad (3.22)$$

The quantization conditions Eq. (3.18) are expanded about the top of the barrier in Appendix B to obtain Eqs. (B13) and (B14), which are

$$\phi_4(R) + \arg\Gamma\left[\frac{1}{2} \mp \frac{1}{4} + i\frac{a(R)}{2}\right]$$

$$-K'(R)a(R) = \pi\left(n + \frac{1}{2} \mp \frac{1}{8}\right), \quad (3.23)$$

where

$$K'(R) = \sqrt{-V''(R;x_T)m}\int_{x_T}^{x_3}\left[\frac{1}{q[V(R;x_T),x]} - \frac{1}{p[V(R;x_T),x]}\right]dx + \frac{1}{4}\ln[mV''(R;x_T)(x_3 - x_T)^4], \quad (3.24)$$

and $\phi_4(R)$ is ϕ_4 of Eq. (3.17) evaluated at $x_2 = x_T$ and $\epsilon = V(R, x_T)$.

Equations (3.22) and (3.23) together with Eq. (3.24) determine energy eigenvalues $\epsilon = \epsilon_T(R)$ near the top-of-barrier energy. Following Demkov [24], we regard $\epsilon(R)$ as a single function of the complex variable R on a Riemann surface with multiple sheets. On the nth sheet along the real R axis, the function $\epsilon(R)$ equals the R-dependent energy eigenvalues $\epsilon_n(R)$. The approximate expression for $\epsilon_T(R)$ is obtained by solving Eqs. (3.23) and (3.24) by iteration. The eigenvalue $\epsilon_T(R)$ is written as

$$\epsilon_T(R) = V(R;x_T) - i\frac{2 \mp 1}{2}\sqrt{\frac{-V''(R;x)}{m}}[1 + 2\delta_A(R)], \quad (3.25)$$

where $\delta_A(R)$ is small quality. A first iteration gives

$$\delta_A^{(0)}(R) = \frac{3 \mp 1}{\sqrt{\pi}}\exp\left\{i2\phi_4(R) + (2 \mp 1)K'(R) \pm i\frac{\pi}{4}\right\}. \quad (3.26)$$

The next iteration gives the value of $\delta_A(R)$ used here

$$\delta_A(R) = \frac{\delta_A^{(0)}(R)}{1 + \delta_A^{(0)}(R)B(R)}, \quad (3.27)$$

where

$$B(R) = \left(2K'(R) + \ln 2 + \gamma - \frac{1}{2} \pm \frac{1}{2}\right). \quad (3.28)$$

Notice that $\epsilon_T(R)$ does not depend upon the quantum number n. This means that all energy eigenvalues corresponding to states with successive values of n connect to the same eigenvalue in the harmonic-oscillator region. For the H_2^+ example, this means that all states of the same symmetry and number of united atom radial nodes join the flat harmonic-oscillator region as seen in Figs. 1 and 2.

The various sheets are joined at branch points R_C. The position of these branch points is determined by

$$\frac{\partial\epsilon_T(R)}{\partial R} \to \infty. \quad (3.29)$$

A smooth path connecting these branch points is determined by Eq. (C9) in Appendix C

$$\mathrm{Im}R = \frac{1}{2}\left\{\frac{\partial\phi_4(R)}{\partial R}\right\}^{-1}\left[(2 \mp 1)K'(\mathrm{Re}R) + 1 - \ln\left(\frac{\sqrt{\pi}}{3 \mp 1}\right) + \ln[B(\mathrm{Re}R)]\right]. \quad (3.30)$$

Along this path joining the branch cuts, the wave function for the system $\Psi(R,x)$ is localized near the top of the barrier. An infinite number of paths connect the branch points, thus, the next task is to select the optimal one.

Classically, a particle that remains exactly at the top of barrier is at rest with respect to this point; thus, its oscillatory motion about this point has an infinite period. This condition is

$$\frac{\partial\phi_4}{\partial\epsilon} \to \infty. \quad (3.31)$$

Owing to the $a\ln|a|$ term in Eq. (3.10), this equation always has a solution at $\epsilon(R) = V(R;x_T)$ independently of the dependence of $V(R;x)$ upon the adiabatic parameter R. This is not true, however, for the quantal phase $\phi_Q = 2(\phi_4 + \phi_0)$. Here the equation

$$\frac{\partial\phi_Q}{\partial\epsilon} \to \infty \quad (3.32)$$

has a solution at $a = i(2 \mp 1)/2$ or $\delta_A = 0$. For most potentials $\delta_A = 0$ requires $\mathrm{Im}R \to \infty$. In this limit the top-of-barrier wave function takes its simplest form, namely, an exponential

$$E(i/2, [-4mV''(R;x_T)]^{1/4}x) = \exp\{(i/4)[-4mV''(R;x_T)]^{1/2}x^2\}. \quad (3.33)$$

The exact form of the path of integration depends upon the details of the potential $V(R;x)$. It must be emphasized that it is not necessary to know the path, since only the function $k_T(R)$ and the end points are needed, and the phase integral is independent of path provided alternate paths can be deformed into each other.

In order to avoid the limit $\mathrm{Im}R \to \infty$, we evaluate $P(E)$ in Eq. (2.14) with $\delta_A(R) \neq 0$. The approximate expression

$$k_T(R) = k_{T0}(R) + \frac{k_T(R)^2 - k_{T0}(R)^2}{k_T(R) + k_{T0}(R)} \approx k_{T0}(R) - M\frac{\epsilon(R) - V(R;x_T)}{k_{T0}(R)} \quad (3.34)$$

is written, using Eq. (3.25) for $\epsilon(R) \approx \epsilon_T(R)$, as

$$k_T(R) = k_{T0}(R) + k_{T1}(R) + k_{T\delta}(R) , \tag{3.35}$$

where

$$k_{T0}(R) = \sqrt{2M[E - V(R; x_T)]} , \tag{3.36}$$

$$k_{T1}(R) = i\frac{2 \mp 1}{2}\frac{M}{k_{T0}(R)}\sqrt{\frac{-V''(R; x_T)}{m}} , \tag{3.37}$$

and

$$k_{T\delta} = 2k_{T1}(R)\delta_A(R) . \tag{3.38}$$

Equation (3.25) has been used in Eqs. (3.35)–(3.38). Note that these expressions are valid only in the region of complex R corresponding to the flat portion of the Riemann surface in Fig. 2. The integral in Eq. (2.14) is now written as

$$\begin{aligned}\mathrm{Im}\int_{R_0}^{\infty} k(R)dR = \mathrm{Im}\int_{R_0}^{R_1}[k_T(R) - k_{T0}(R)]dR \\ +\mathrm{Im}\int_{R_1}^{\infty}[k(R) - k_{T0}(R)]dR.\end{aligned} \tag{3.39}$$

The approximation Eq. (3.35) for $k_T(R)$ is then employed in the second integral so that Eq. (3.39) becomes, after some rearrangement of terms,

$$\begin{aligned}\mathrm{Im}\int_{R_0}^{\infty} k_T(R)dR = \mathrm{Im}\int_{R_0}^{R_1}[k_T(R) - k_{T0}(R) \\ -k_{T1}(R) - k_{T\delta}(R)]dR \\ +\mathrm{Im}\int_{R_0}^{\infty} k_{T1}(R)dR \\ +\mathrm{Im}\int_{R_0}^{\infty} k_{T\delta}(R)dR.\end{aligned} \tag{3.40}$$

Corresponding to this decomposition of $k(R)$, there is the factorization of $P(E)$

$$P(E) = P_0(E)P_\delta(E)P_\infty(E) , \tag{3.41}$$

where

$$\begin{aligned}P_0(E) = \exp\Bigg\{-2\,\mathrm{Im}\int_{R_0}^{R_1}[k_T(R) \\ -k_{T0}(R) - k_{T1}(R) - k_{T\delta}]dR\Bigg\} ,\end{aligned} \tag{3.42}$$

$$P_\delta(E) = \exp\left[-2\,\mathrm{Im}\int_{R_0}^{\infty} k_{T\delta}(R)dR\right] , \tag{3.43}$$

$$P_\infty(E) = \exp\left[-2\,\mathrm{Im}\int_{R_0}^{\infty} k_{T1}(R)dR\right] , \tag{3.44}$$

and the point R_1 is determined by the condition $\delta_A(R) << 1$. Our derivation shows that the integrals in Eqs. (3.43) and (3.44) are taken along a path that passes through R_1 in the complex plane. Because $k_{T\delta}(R)$ and $k_{T1}(R)$ are analytic functions of R, this path can be deformed to go along the real axis.

Since $\delta_A(R)$ is a strongly oscillating function on the real axis, the integral in $P_\delta(E)$ is accurately evaluated by the stationary phase method. Using

$$\phi_4(R) \approx \phi_4(R_0) + \left.\frac{\partial\phi_4(R)}{\partial R}\right|_{R_0}(R - R_0) , \tag{3.45}$$

we obtain

$$P_\delta(E) = \exp\left\{-4\,\mathrm{Im}\delta_A(R_0)\left[\left.\frac{\partial\phi_4(R)}{\partial R}\right|_{R_0}\right]^{-1} k_{T1}(R_0)\right\} . \tag{3.46}$$

We set $R_0 = \mathrm{Re}R_C$ so that $\mathrm{Im}\delta_A^{(1)}(R_0) = \mathrm{Im}\delta_A^{(0)}(R_0) = 0$, which gives $P_\delta(E) = 1$. Thus, we see that $P(E)$ is written as the product of two factors, namely, a factor, $P_0(E)$, that pertains to the region between R_0 and R_1, and a factor, $P_\infty(R)$, that pertains to the region from R_0 to infinity. Since $k_{T1}(R)$ is analytic, the integral in $P_\infty(R)$ may be taken along the real axis. Along the real axis $k_{T1}(R)$ is purely imaginary so that we have the simple expression

$$P_\infty(E) = \exp\left[-(2 \mp 1)\int_{R_0}^{\infty}\sqrt{\frac{-MV''(R; x_T)}{2m[E - V(R, x_T)]}}dR\right] , \tag{3.47}$$

and $P_0(E)$ is given by Eq. (3.42).

The eigenfunctions and energy eigenvalues are those of a harmonic oscillator, while along the real axis they represent Rydberg states. The curve given by the locus of branch points Eq. (3.30) separates the complex R plane into two regions, one where the eigenvalues have mainly a Rydberg structure, and one where the eigenvalues are harmonic-oscillator-like, as illustrated in Fig. 4. In the latter region the harmonic-oscillator struc-

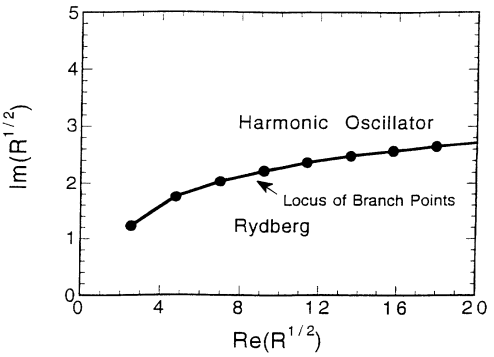

FIG. 4. Plot of the locus of branch points in the complex $\sqrt{R}$ plane. The smooth curve joining the points separates the plane into a part for which the eigenvalue spectrum is Rydberg-like and a region where the spectrum is harmonic-oscillator-like.

ture emerges because the wave functions Eq. (3.33) for $\mathrm{Im}R > \sqrt{\mathrm{Re}R}\ln(\mathrm{Re}R)$ are confined to the top-of-barrier region. The confinement of the electron wave function to the top-of-barrier region represents a key advantage of integrating the Schrödinger equation along a path in the complex R plane.

IV. APPLICATIONS

For proton-hydrogen collisions the relevant potential $V_a(R,\mathbf{r})$ is that of an electron moving in the field of two positive ions. The model potential has electron coordinates perpendicular to the internuclear axis set equal to zero and the scaled coordinate along this axis denoted by x. The origin is at the top of the barrier so that $x_T = 0$. There is also a term [21]

$$\frac{1}{2}R\ddot{R}x^2 = -\frac{1}{2}\frac{R}{M}\frac{dV_a(R;x_T)}{dR}x^2\,, \tag{4.1}$$

where $\ddot{R}$ denotes the second derivative of R with respect to time and we have used the relation

$$dt = dR/v(R) = MdR/k_{T0}(R)\,. \tag{4.2}$$

Thus, we have for the effective potential $V(R,x)$

$$V(R;x) = V_a(R;x) - \frac{1}{2}\frac{R}{M}\frac{dV(R;x_T)}{dR}(x-x_T)^2, \tag{4.3}$$

where

$$V_a(R;x) = -\frac{1}{R}\left(\frac{Z_1}{|1/2-x|} + \frac{Z_2}{|1/2+x|}\right) + \frac{Z_1Z_2}{R}$$

and

$$x_T = \frac{1}{2}\frac{Z_2^{\frac{1}{2}} - Z_1^{\frac{1}{2}}}{Z_2^{\frac{1}{2}} + Z_1^{\frac{1}{2}}}\,.$$

For this potential, the quantities in Eq. (3.47) are

$$V(R;x_T) = -C_0/R\,, \tag{4.4}$$

where

$$C_0 = \left(Z_2^{\frac{1}{2}} + Z_1^{\frac{1}{2}}\right)^2 - Z_1Z_2\,,$$

and

$$V''(R;x_T) = -\frac{C_1}{R} - \frac{C_0}{MR}\,, \tag{4.5}$$

where

$$C_1 = \frac{2\left(Z_2^{\frac{1}{2}} + Z_1^{\frac{1}{2}}\right)^4}{Z_1^{\frac{1}{2}}Z_2^{\frac{1}{2}}}\,.$$

Recalling that $m = m_0R^2$, where m_0 is the reduced mass of the electron relative to the center of mass of the two protons, substituting Eqs. (4.4) and (4.5) into Eq. (3.47) and setting $y_0 = ER_0/C_0$ gives for g states

$$P_\infty(E) = \exp\left[-\sqrt{\frac{C_1M}{2C_0m_0} + \frac{1}{2}}\int_{y_0}^{\infty}\frac{dy}{y\sqrt{y+1}}\right] \tag{4.6}$$

$$= \exp\left[\zeta_{\mathrm{ad}}\ln\left(\frac{\sqrt{y_0+1}-1}{\sqrt{y_0+1}+1}\right)\right], \tag{4.7}$$

where

$$\zeta_{\mathrm{ad}} = \sqrt{\frac{C_1M}{2C_0m_0} + \frac{1}{2}} \tag{4.8}$$

is an approximate value of the Wannier index, as we show later.

For $E \gg C_0/R_0$ the argument of the ln function in Eq. (4.7) can be expanded in powers of $1/\sqrt{y_0}$ to give

$$P_\infty(E) \approx \exp[-2\zeta_{\mathrm{ad}}/\sqrt{y_0}] = \exp[-\Delta/v], \tag{4.9}$$

where

$$\Delta = \sqrt{C_1/m_0 + C_0/M}/\sqrt{R_0}, \tag{4.10}$$

and $v = \sqrt{2E/M}$ is the relative velocity of the like charged particles in the final state. This agrees with the expression used in Ref. [19] to compute ionization in H^++H collisions at low to intermediate energies.

Near the threshold for ionization, where $E \ll C_0/R_0$, the argument of the ln function in Eq. (4.7) is approximately equal to $y_0/4$ and one has

$$\exp\left[\zeta_{\mathrm{ad}}\ln\left(\frac{\sqrt{y_0+1}-1}{\sqrt{y_0+1}+1}\right)\right]$$

$$\approx \exp[\zeta_{\mathrm{ad}}\ln(y_0/4)]$$

$$= \exp\zeta_{\mathrm{ad}}\{\ln E - \ln[R_0/4(C_0)]\}, \tag{4.11}$$

from which it follows that

$$\sigma \propto E^{\zeta_{\mathrm{ad}}}. \tag{4.12}$$

This expression for the ionization cross section has the same form as the Wannier threshold law, however, the exponent is ζ_{ad} rather than ζ. Comparison with Feagin's [7] expression for ζ, namely,

$$\zeta = \sqrt{\frac{C_1M}{2C_0m_0} + \frac{9}{16}} - \frac{1}{4}\,, \tag{4.13}$$

shows that ζ_{ad} differs from the correct index ζ. The relation between these two indices can be written

$$\zeta_{\mathrm{ad}} = \zeta\sqrt{1 + 1/2\zeta}\,. \tag{4.14}$$

For proton-hydrogen collisions, where the value of ζ equals 69.7, the error in ζ_{ad} is negligible, but even this small error means that the "adiabatic" theory does not give the correct zero velocity limit of the ionization cross section. Aside from this small error, Eq. (4.7) gives an expression for the ionization probability that connects the Wannier threshold region with the keV energy region. In this latter region the cross section has been compared favorably with measurements. Measurements between the keV and the threshold region are needed to further test Eq. (4.7).

For ionization of hydrogen by electron impact, ζ equals 1.127 and here the error in $\zeta_{\rm ad}$ is of the order of 23%, an unacceptably large value. This shows that diabatic corrections are needed in order to obtain the correct zero velocity limit of ionization cross sections, even when the Schrödinger equation is integrated along an optimal path in the complex R plane.

A first diabatic correction to the adiabatic Wannier index is computed in Appendix D. The cross section has a power-law dependence with an index $\zeta^{(1)}$ given by Eq. (D11)

$$\zeta^{(1)} = \zeta_{\rm ad}\left(1 - \frac{1}{4}\frac{1}{\zeta_{\rm ad}+1/4}\right) \approx \zeta_{\rm ad} - \frac{1}{4} + \frac{1}{16\zeta_{\rm ad}} . \quad (4.15)$$

This is to be compared with the corresponding expression for the Wannier index ζ,

$$\zeta \approx \zeta_{\rm ad} - \frac{1}{4} + \frac{1}{32\zeta_{\rm ad}} . \quad (4.16)$$

It is apparent that $\zeta^{(1)}$ very closely approximates the full diabatic result. Even for the ionization of hydrogen by electrons, the error in $\zeta^{(1)}$ is of the order of 2%, indicating that the adiabatic approximation with a first diabatic correction accurately represents the propagation of top-of-barrier wave functions along a path in the complex plane which goes to the left of the branch points shown in Fig. 4. It is also apparent that the $v \to 0$ limit is not given by the adiabatic approximation along this same path. This observation has important implications for the low velocity limit of reaction cross sections. Theorems stating that the $v \to 0$ limit is given by adiabatic approximations must also implicitly take $M \to \infty$. The accurate value that obtains for the Wannier index with a first diabatic correction to the adiabatic value also shows that the harmonic-oscillator term in the potential that Solov'ev and Vinitsky [21] derive is essential for a correct determination of the Wannier index.

To complete the computation of ionization cross sections it is necessary to evaluate $P_0(E)$. This requires computing R_1 consistent with the condition that the analytic approximation to $\epsilon_T(R)$ accurately approximates the numerically computed $\epsilon(R)$. Since the numerically computed $\epsilon(R)$ omits the dynamical oscillator potential in $V(R;x)$, its effects must also be omitted in the approximate $\epsilon_T(R)$ for purposes of computing R_1. We found, however, that a very large value of R was necessary in order to match $\epsilon_T(R)$ from Eq. (3.24) with $\epsilon(R)$. For that reason an expression for $\epsilon_T(R)$, including terms of order R^{-2} and $R^{-5/2}$, was computed. These terms arise from anharmonic corrections to the harmonic top-of-barrier potential. Then it was found possible to match the analytic expression to the numerical $\epsilon(R)$ at $R_1 \approx 200$ a.u. The anharmonic terms should also be included in the computation of $P_\infty(E)$ in order to have a consistent theory. When this is done we find that $P_\infty(E)$ for small E no longer has the Wannier form, $E^\zeta f(E)$, where $f(E)$ is analytic in E; rather we find that $f(E)$ includes terms of order $\sqrt{E}$ and $E\ln E$. The details of the computation are given in Appendix E. These purely adiabatic results are combined with the higher-order diabatic corrections to give a new expression for $P_\infty(E)$. Using Eqs. (E8) and (E9) in Eq. (E3) with the constants C_0, C_1', and C_1 replaced by their diabatic values gives

$$P_\infty(E) = E^{\zeta^{(1)}} \exp\zeta^{(\rm ad)}\left[-\sqrt{3E} - \frac{13}{64}E\ln E + \left(\frac{153}{128} - \ln 3\right) + E\left(\frac{25}{192} + \frac{13}{64}\ln 3\right)\right], \quad E \ll 1 \quad (4.17)$$

$$P_\infty(E) = \exp\left[-\frac{93\sqrt{2}}{32v}\right], \quad E > 1. \quad (4.18)$$

Note that the coefficient of $E^{\zeta^{(1)}}$ in Eq. (4.17) is not analytic in E near $E = 0$. More importantly Eq. (4.17) shows that these coefficients are independent of R_1; thus, they represent corrections that come from the asymptotic region. It must be emphasized that these corrections do not include effects of rotation.

The form of the anharmonic contributions to $P_\infty(E)$ is unexpected. In contrast, the function $P_0(E)$ pertaining to the inner region is analytic in E, although the expression must be evaluated numerically. We find

$$P_0(E) = \exp[-(0.94 - 0.6E)\sqrt{M/m_0}], \quad E \to 0 \quad (4.19)$$

and

$$P_0(E) = \exp[-1.0/v], \quad E > 1. \quad (4.20)$$

V. EXTENSIONS AND CONNECTIONS WITH OTHER THEORIES

Figure 2(a) shows that by integrating the Schrödinger equation along a path in the complex plane, the Rydberg structure of energy levels on the real axis joins with a region where the wave function is localized on the top of the barrier. This localization occurs because the top-of-barrier wave function for complex R has an exponentially decreasing part given by

$$\exp[-B\,{\rm Im}\sqrt{R}\,x^2] , \quad (5.1)$$

where B is a constant equal to $(1/2)\sqrt{[32Z - (4Z-1)/M]m_0}$. Equation (C11) shows that the imaginary part of $\sqrt{R}$ is proportional to $\ln({\rm Re}R)$, thus, as R increases, the functions become localized on the top of the barrier near $x = x_T = 0$, and the imaginary part of the adiabatic eigenvalues correspond to those of a harmonic oscillator. The corresponding eigenfunctions are harmonic-oscillator functions with $a = (n_{\rm osc} + 1/2)i$. It is possible to connect excited states on the real axis with those in the large R region by integrating along sheets corresponding to $n \neq 0$. The corresponding threshold law has a larger index $(2n_{\rm osc}+1)\zeta^{(1)}$ appropriate for the particular oscillator quantum number $n_{\rm osc}$. The value of $n_{\rm osc}$ is set by the initial conditions;

thus, if the initial state is antisymmetric about the point $x = 0$, then the lowest mode has an index that is three times larger than the index for a symmetric state, as is evident already in Eq. (3.47). Thus, triplet S states of $e^- + H$ have a Wannier index equal to $3 \times 1.127 = 3.381$ in agreement with the value obtained by Feagin [7]. Depending upon the initial state, a threshold behavior with and index equal to $(2n_{\rm osc} + 1)\zeta$ is possible.

Motion perpendicular to the internuclear axis has not been considered in this work except in the anharmonic corrections of Appendix E. Such motion is represented by bound harmonic-oscillator functions near the top of the barrier. Since the motion is bound for both real and complex R, it affects the real part of $\epsilon_T(R)$ and therefore does not alter threshold laws but does affect angular distributions. Consideration of general wave-function propagation leads to diabatic representations of the propagator for time-dependent harmonic oscillators as discussed, for example, by Jakubassa-Amundsen and Macek [14] and Macek [16]. Harmonic-oscillator states for time-dependent potentials have also been discussed by Kazansky and Ostrovsky [20], who emphasize real values of R.

A key assumption of the Wannier's original theory is that electrons which move away from the top-of-barrier fall into Rydberg states and do not lead to ionization. In quantal versions of this theory where wave function propagation is confined to the real axis, it is necessary to employ perfectly absorbing boundary conditions at some unspecified boundary in order to incorporate Wannier's assumption. This additional assumption is not needed in the present approach because the wave function is concentrated on the top of the barrier for appropriate integration paths in the complex R plane. The adiabatic framework used here, thus, provides a new perspective on this controversial assumption of Wannier's theory.

A related aspect of the present theory is that it is, in principle, possible to compute absolute cross sections as done in Sec. V for proton impact on atomic hydrogen. To do this for electron impact, more complete formulations incorporating angular motion and exact numerical hyperspherical eigenvalues for complex R in the reaction zone are needed. There are no fundamental difficulties involved in finding such eigenvalues, but this is a task that goes beyond the scope of the present manuscript.

It is also possible to compute excitation to Rydberg states using the present theory. If a path joining with a sheet corresponding to a Rydberg state is chosen, then $P(E)$ in Eq. (2.14) gives the probability for exciting a particular Rydberg state. This represents a possible avenue for further work, but requires numerical calculations of $\epsilon(R)$. In addition, it is necessary to include diabatic corrections as has been done here for ionization.

The adiabatic threshold law for proton-hydrogen collisions was obtained earlier [18], but yielded a slightly different result, namely, $\sigma \propto (E/\ln^4 E)^{\zeta_{\rm ad}}$. The $\ln E$ factor is now regarded as erroneous. It appears upon integrating along a path which passes very close to the branch points. The energy eigenvalues are not smooth functions of R along this path; thus, a smoothed function $\epsilon(R)$ was employed in Ref. [18] to evaluate the integral in Eq. (2.14). Apparently, the integral with the smoothed function does not represent the actual integral with sufficient accuracy. Figure 2 shows that $\epsilon(R)$ is smooth along paths which are well removed from the branch cuts. Along these paths accurate analytic evaluations are easily performed, as we have shown.

VI. CONCLUSIONS

We have analyzed the ionization of H atoms by charged particles employing an adiabatic approximation in the complex R plane. Exact energy eigenvalues of $H_2{}^+$ for complex R are computed to illustrate the simplification that occurs in the eigenvalue spectrum in certain regions in the complex R plane. General expressions for top-of-barrier eigenvalues are derived using semiclassical and comparison equation methods. Along the best path in the complex R plane, the eigenvalues and eigenfunctions are those of a harmonic oscillator with a complex spring constant corresponding to electron motion on the top of the potential barrier between the two protons. By integrating the Schrödinger equation along this best path, an expression for the ionization cross section is obtained that connects the threshold and keV regions of proton energy. It is shown that the adiabatic theory gives an incorrect Wannier exponent for the threshold cross section, but that a first diabatic correction gives an exponent that closely approximates the Wannier exponent. The theory is also shown to yield Wannier exponents for the ionization of hydrogen by electrons that are within 2% of the accepted values for ionization into ^1S and ^3S continuum states.

ACKNOWLEDGMENTS

This manuscript grew out of discussions at the Harvard-Smithsonian Institute for Theoretical Atomic and Molecular Physics Workshop and at the Santa Barbara Institute for Theoretical Physics project on time-dependent phenomena. Discussion with the project director, the late Chris Bottcher, were particularly helpful. Support for collaboration with the Ioffe Physical Technical Institute, St. Petersburg, Russia is provided by the National Science Foundation under Grant No. PHY-9213953. This research was sponsored by the Division of Chemical Sciences, U.S. Department of Energy, under Contract No. DE-AC05-84OR21400 managed by Martin Marietta Energy System, Inc.

APPENDIX A: QUANTIZATION CONDITIONS FOR TOP-OF-BARRIER MOTION

Quantization conditions emerge by joining wave functions in classically allowed regions with wave functions in classically forbidden regions. This requires that the phase in the allowed region equals an odd multiple of $\pi/2$. For the potential used here this phase is just the phase of $\psi_{\rm IV}$ given by Eq. (3.15), which can be written

$$\phi_4(x) + \phi_0 + \arctan\left[\frac{1-A}{1+A}\tan(\phi_2 + \phi_0)\right] - \pi/4. \quad \text{(A1)}$$

Upon joining to the usual WKB solution in region V, we obtain the semiclassical quantization condition for the eigenvalues of $\mathcal{H}(R;x)$

$$\phi_4+\phi_0+\arctan\left[\frac{1-A}{1+A}\tan(\phi_2+\phi_0)\right]=(n+1/2)\pi, \tag{A2}$$

where $\phi_4=\phi_4(x_3)$. This equation may be written in a form which exhibits the symmetry in ϕ_4 and ϕ_2

$$\arctan\left[\frac{A\sin(\phi_4-\phi_2)+\sin(\phi_4+\phi_2+2\phi_0)}{A\cos(\phi_4-\phi_2)+\cos(\phi_4+\phi_2+2\phi_0)}\right]=(n+1/2)\pi. \tag{A3}$$

Since Eq. (A3) holds only when

$$A\cos(\phi_4-\phi_2)+\cos\phi=0\,, \tag{A4}$$

where

$$\phi=\phi_4+\phi_2+2\phi_0\,, \tag{A5}$$

the quantization condition may be written

$$\phi\pm\arccos\left[A\cos(\phi_4-\phi_2)\right]=\pi(2n+1)\,. \tag{A6}$$

For symmetric potentials the eigenfunctions are even "g" or odd "u" under reflection, and it is convenient to write the quantization conditions explicitly for each case. For this purpose the two equations from Abramowitz and Stegun [27]

$$\Gamma(2z)=\frac{1}{2\sqrt{\pi}}2^{2z}\Gamma(z)\,\Gamma\left(z+\frac{1}{2}\right) \tag{A7}$$

and

$$\Gamma(z)\,\Gamma(1-z)=\frac{\pi}{\sin(\pi z)} \tag{A8}$$

are used. Substituting $z=\frac{1}{4}\pm i\frac{a}{2}$ into Eqs. (A7) and (A8) gives

$$\Gamma\left(\frac{1}{2}+ia\right)=\frac{1}{2\sqrt{\pi}}2^{\frac{1}{2}\pm ia}\Gamma\left(\frac{1}{4}\pm i\frac{a}{2}\right)\Gamma\left(\frac{3}{4}\pm i\frac{a}{2}\right) \tag{A9}$$

and

$$\arg\Gamma\left(\frac{1}{4}\pm i\frac{a}{2}\right)\arg\Gamma\left(\frac{3}{4}\mp i\frac{a}{2}\right)=\frac{\pi}{\sin\left(\frac{\pi}{4}\pm i\frac{\pi a}{2}\right)}\,. \tag{A10}$$

Using the analytic continuation of $\arg\Gamma\left(\frac{1}{2}+iz\right)$ to complex z

$$\arg\Gamma\left(\frac{1}{2}+iz\right)=-\frac{i}{2}\ln\frac{\Gamma\left(\frac{1}{2}+iz\right)}{\Gamma\left(\frac{1}{2}-iz\right)}\,, \tag{A11}$$

together with (A9) and (A10) gives

$$\begin{aligned}\arg\Gamma\left(\frac{1}{2}+ia\right)&=-\frac{i}{2}\ln\frac{\Gamma\left(\frac{1}{2}+ia\right)}{\Gamma\left(\frac{1}{2}-ia\right)}\\&=-\frac{i}{2}\ln\left[2^{i2a}\frac{\Gamma\left(\frac{1}{4}+i\frac{a}{2}\right)}{\Gamma\left(\frac{1}{4}-i\frac{a}{2}\right)}\frac{\Gamma\left(\frac{3}{4}+i\frac{a}{2}\right)}{\Gamma\left(\frac{3}{4}-i\frac{a}{2}\right)}\right]\\&=\arg\Gamma\left(\frac{1}{4}+i\frac{a}{2}\right)+\arg\Gamma\left(\frac{3}{4}+i\frac{a}{2}\right)+a\ln 2\end{aligned} \tag{A12}$$

and

$$\begin{aligned}\arg\Gamma\left(\frac{1}{4}+i\frac{a}{2}\right)-\arg\Gamma\left(\frac{3}{4}+i\frac{a}{2}\right)&=-\frac{i}{2}\ln\frac{\Gamma\left(\frac{1}{4}+i\frac{a}{2}\right)\Gamma\left(\frac{3}{4}-i\frac{a}{2}\right)}{\Gamma\left(\frac{1}{4}-i\frac{a}{2}\right)\Gamma\left(\frac{3}{4}+i\frac{a}{2}\right)}\\&=-\frac{i}{2}\ln\frac{\sin\left(\frac{\pi}{4}-i\frac{\pi a}{2}\right)}{\sin\left(\frac{\pi}{4}+i\frac{\pi a}{2}\right)}\\&=\frac{i}{2}\ln\left[\tan\left(\frac{\pi}{4}-i\frac{\pi a}{2}\right)\right]\\&=\arctan\left(e^{-\pi a}\right)-\frac{\pi}{4}=\arccos A-\frac{\pi}{4}\,.\end{aligned} \tag{A13}$$

The definition of $\arctan(z)$ for complex z, namely,

$$\arctan z=\frac{i}{2}\ln\left[\tan\left(\frac{i}{2}\ln z+\frac{\pi}{4}\right)\right]+\frac{\pi}{4} \tag{A14}$$

has been used in Eq. (A13). Summing Eqs. (A12) and (A13) gives

$$\arg\Gamma\left(\frac{1}{2}+ia\right)+\arccos A-\frac{\pi}{4}=\arg\Gamma\left(\frac{1}{4}+i\frac{a}{2}\right)+a\ln 2\,, \tag{A15}$$

while subtracting them gives

$$\arg\Gamma\left(\frac{1}{2}+ia\right)-\arccos A+\frac{\pi}{4}=\arg\Gamma\left(\frac{3}{4}+i\frac{a}{2}\right)+a\ln 2\,. \tag{A16}$$

These equations are equivalent to the single relation

$$\arg\Gamma\left(\frac{1}{2}+ia\right)=2\arg\Gamma\left(\frac{1}{2}\mp\frac{1}{4}+i\frac{a}{2}\right)+a\ln 2\mp\left(\arccos A-\frac{\pi}{4}\right)\,, \tag{A17}$$

where "−" refers to "g" and "+" to "u" eigenstates. For symmetric potentials the quantization Eq. (A6) becomes

$$2(\phi_4+\phi_0)\pm\arccos A=\pi(2n+1)\ . \tag{A18}$$

Substituting (A17) into the definition Eq. (3.10) of ϕ_0 and the result into Eq. (A18) gives the quantization condition

$$\phi_4+\arg\Gamma\left(\frac{1}{2}\mp\frac{1}{4}+i\frac{a}{2}\right)+\frac{a}{2}\left(1-\ln\frac{|a|}{2}\right)=\pi\left(n+\frac{1}{2}\mp\frac{1}{8}\right)\ . \tag{A19}$$

APPENDIX B: EXPANSION OF $\epsilon(R)$ AROUND THE TOP-OF-BARRIER ENERGY

Equation (3.18) applies for all values of the energy ϵ. Numerically, however, these expressions are inconvenient near the top-of-barrier energy $\epsilon_0=V(R;x_T)$. For this purpose it is useful to expand the quantization conditions about ϵ_0. In order to expand ϕ_4, for example, it is convenient to employ a more complete notation for q, namely, $q(\epsilon,x)$,

$$q(\epsilon,x)=\sqrt{2m[\epsilon-V(R;x)]} \tag{B1}$$

and a comparison expression $p(\epsilon,x)$ equal to $q(\epsilon,x)$ at the top-of-barrier $x-x_T$

$$p(\epsilon,x)=\sqrt{2m\left[\epsilon-V(R;x_T)-\frac{1}{2}V''(R;x_T)(x-x_T)^2\right]}\ , \tag{B2}$$

where $\epsilon-V(R;x_T)>0$. Further, we define

$$\phi_4(\epsilon)=\int_{x_T}^{x_3}q(\epsilon,x)dx. \tag{B3}$$

Using the identity

$$\begin{aligned}q(\epsilon,x)&=q(\epsilon_0,x)+q(\epsilon,x)-q(\epsilon_0,x)\\&=q(\epsilon_0,x)+[q^2(\epsilon,x)\\&\quad-q^2(\epsilon_0,x)]/[q(\epsilon,x)+q(\epsilon_0,x)]\ ,\end{aligned} \tag{B4}$$

and adding and subtracting a term $1/[p(\epsilon,x)+p(\epsilon_0,x)]$ gives

$$\phi_4(\epsilon)=\phi_4(\epsilon_0)+2m(\epsilon-\epsilon_0)\int_{x_T}^{x_3}\left[\frac{1}{q(\epsilon,x)+q(\epsilon_0,x)}-\frac{1}{p(\epsilon,x)+p(\epsilon_0,x)}\right]dx+2m(\epsilon-\epsilon_0)\int_{x_T}^{x_3}\frac{dx}{p(\epsilon,x)+p(\epsilon_0,x)} \tag{B5}$$

$$\begin{aligned}&=\phi_4(\epsilon_0)+2m(\epsilon-\epsilon_0)\int_{x_T}^{x_3}\left[\frac{1}{q(\epsilon,x)+q(\epsilon_0,x)}-\frac{1}{p(\epsilon,x)+p(\epsilon_0,x)}\right]dx\\&\quad+\frac{m(\epsilon-\epsilon_0)}{\sqrt{-mV''(R;x_T)}}[-y^2+y\sqrt{1+y^2}+\ln(y+y\sqrt{y^2+1})]|_{x_T}^{x_3},\end{aligned} \tag{B6}$$

where

$$y=(x_3-x_T)\sqrt{\frac{-V''(R;x_T)}{2(\epsilon-\epsilon_0)}}\ . \tag{B7}$$

This expression is to be evaluated near $\epsilon\approx\epsilon_0$. In this region

$$a\approx\sqrt{\frac{m}{-V''(R;x_T)}}(\epsilon_0-\epsilon)\ , \tag{B8}$$

and one has, to first order in $\epsilon-\epsilon_0$, the result

$$\phi_4(\epsilon)=\phi_4(\epsilon_0)+K_4(\epsilon-\epsilon_0)-\frac{a}{2}(1-\ln|a|), \tag{B9}$$

where

$$K_4=m\int_{x_T}^{x_3}\left[\frac{1}{q(\epsilon_0,x)}-\frac{1}{p(\epsilon_0,x)}\right]dx+\frac{1}{2}\sqrt{\frac{m}{-V''(R;x_T)}}\times\ln[2p(\epsilon_0,x_3)(x_3-x_T)]. \tag{B10}$$

A similar expression holds for ϕ_2; thus, we may write for ϕ the expression

$$\phi_4+\phi_2+2\phi_0\approx\int_{x_1}^{x_3}q(\epsilon_0,x)dx+K(\epsilon-\epsilon_0)+\arg\Gamma[1/2+ia], \tag{B11}$$

where

$$K=m\int_{x_1}^{x_3}\left[\frac{1}{q(\epsilon_0,x)}-\frac{1}{p(\epsilon_0,x)}\right]dx+\frac{1}{2}\sqrt{\frac{m}{-V''(R;x_T)}}\times\ln[4p(\epsilon_0,x_3)(x_3-x_T)p(\epsilon_0,x_1)(x_T-x_1)]\ . \tag{B12}$$

Substituting $\epsilon-\epsilon_0$ from Eq. (B8) into Eq. (B9) and the result into Eq. (3.18) specializing to the symmetric case and defining a new constant K' as

$$K'(R)=\sqrt{-V''(R;x_T)m}\int_{x_T}^{x_3}\left[\frac{1}{q[V(R;x_T),x]}-\frac{1}{p[V(R;x_T),x]}\right]dx+\frac{1}{4}\ln[mV''(R;x_T)(x_3-x_T)^4] \tag{B13}$$

gives

$$\phi_4(R) + \arg\Gamma\left[\frac{1}{2} \mp \frac{1}{4} + i\frac{a(R)}{2}\right] - K'(R)a(R) = \pi\left(n + \frac{1}{2} \mp \frac{1}{8}\right) , \quad \text{(B14)}$$

where

$$a(R) \approx \sqrt{\frac{m}{-V''(R;x_T)}}[V(R;x_T) - \epsilon] , \quad \text{(B15)}$$

and the dependence of a and ϵ upon R is shown explicitly. Equations (B14) and (B15) determine $\epsilon_T(R)$.

APPENDIX C: LOCATION OF TOP-OF-BARRIER BRANCH POINTS

The branch points separate the harmonic-oscillator region from Rydberg valley. The harmonic-oscillator region corresponds to values of $a(R) = [V(R;x_T) - \epsilon(R)]\sqrt{-m/V''(R;x_T)}$, which lie close to those for which the parabolic cylinder functions are simple exponentials, i.e., to values of $a(R)$ near $i(2 \mp 1)/2$. Substituting $a(R) = i[(2 \mp 1)/2 + \delta_A(R)]$ into Eq. (3.23) and dropping terms of order δ_A^2, we get the equation for δ_A

$$F_\pm(R, \delta_A) = \pi(n + 1 \mp 1/8) , \quad \text{(C1)}$$

where

$$F_\pm(R,y) = \phi_4(R) - \frac{i}{2}\left[(2 \mp 1)K'(R) - \ln\left(\frac{\sqrt{\pi}}{3 \mp 1}\right) - \ln y + B(R)y\right], \quad \text{(C2)}$$

$$B(R) = \left(2K'(R) + \ln 2 + \gamma - \frac{1}{2} \pm \frac{1}{2}\right), \quad \text{(C3)}$$

and $\gamma = 0.5772$ is the Eulerian constant.

The various sheets of the function $\epsilon(R)$ are joined at branch points R_C. At the branch points the function $\partial\epsilon(R)/\partial R$ has a singularity

$$\frac{\partial\epsilon(R)}{\partial R} \to \infty \quad \text{when} \quad R \to R_C . \quad \text{(C4)}$$

This condition is equivalent to

$$\frac{\partial F_\pm(R_C, \delta)}{\partial\delta} = 0 . \quad \text{(C5)}$$

Equation (C5) has a solution δ_B,

$$\delta_B(R_C) = B(R_C)^{-1} . \quad \text{(C6)}$$

Equation (C1) determines δ_A for all R and n, while Eq. (C5) determines δ_B for $R = R_C$. The values of R_C corresponding to different n occur at specific points in the complex R plane for which $\delta_B(R_C) = \delta_A(R_C)$. Using this identity and Eq. (C6) in Eq. (C1) gives an implicit equation for R_C

$$\phi_4[V(R_C;x_T)] - \frac{i}{2}\left[(2 \mp 1)K'(R_C) + 1 - \ln\left(\frac{\sqrt{\pi}}{3 \mp 1}\right) + \ln[B(R_C)]\right] = \pi\left(n + 1 \mp \frac{1}{8}\right) . \quad \text{(C7)}$$

In the present case $\mathrm{Re}R_C > \mathrm{Im}R_C$, then $\mathrm{Re}R_C$ is determined by

$$\phi_4[V(R_C;x_T)] = \pi(n + 1 \mp 1/8) + O(\mathrm{Im}R_C/\mathrm{Re}R_C), \quad \text{(C8)}$$

and $\mathrm{Im}R$ is given by

$$\mathrm{Im}R_C = \frac{1}{2}\left\{\left.\frac{\partial\phi_4(R)}{\partial R}\right|_{\mathrm{Re}R_C}\right\}^{-1}\left[(2 \mp 1)K'(\mathrm{Re}R_C) + 1 - \ln\left(\frac{\sqrt{\pi}}{3 \mp 1}\right) + \ln[B(\mathrm{Re}R_C)]\right] . \quad \text{(C9)}$$

A smooth path connecting these branch points is given by Eq. (C9) with R_C replaced by a continuous variable R.

For g states of H_2^+ the quantities in Eqs. (C8), (C9), and (3.25) are

$$\begin{aligned} V(R,x_T) &= -\frac{3}{R} , \\ V''(R,x_T) &= -\frac{32}{R} , \\ \phi_4(R) &= \sqrt{2R} , \\ K'(R) &= \frac{1}{4}\ln(32R) - 1 , \\ B(R) &= \frac{1}{2}\ln R + \frac{7}{2}\ln 2 - 2 + \gamma , \\ \delta_A^{(0)}(R) &= \frac{4}{e\sqrt{\pi}}(2R)^{\frac{1}{4}}\exp(i2\sqrt{2R} + i\pi/4) , \end{aligned} \quad \text{(C10)}$$

so that Eq. (C9) becomes

$$\mathrm{Im}R = \frac{1}{2}\sqrt{2\mathrm{Re}R}\left[\frac{1}{4}\ln\mathrm{Re}R + \ln\left(\frac{12}{2^{1/4}\pi^{1/2}}\right) + \ln\left(\frac{1}{2}\ln\mathrm{Re}R + \frac{7}{2}\ln 2 - 2 + \gamma\right)\right] . \quad \text{(C11)}$$

This result agrees, to lowest order in R, with Pieksma and Ovchinnikov [19] who compute the position of these T-series branch points for H_2^+ and find

$$\mathrm{Im}R_C = \frac{1}{8}\sqrt{2\mathrm{Re}R_C}\ln\mathrm{Re}R_C \quad \text{(C12)}$$

with $\mathrm{Re}R_C = (\pi n)^2/2$.

APPENDIX D: DIABATIC CORRECTIONS TO THE ADIABATIC WANNIER INDEX

To see how diabatic corrections are included at low energy, consider that the standard Wannier theory employs the approximations used in Eqs. (2.12) and (3.34) by expanding the operator $\hat{k}(R)$ about top-of-barrier point x_T

$$\hat{k}(R) \approx k_{T0}(R) + (M/k_{T0})\left[-\frac{1}{2m}\frac{d^2}{dx^2} + \frac{1}{2}V''(R;x_T)x^2\right], \tag{D1}$$

where k_{T0} is given by Eq. (3.37). The approximate Schrödinger equation

$$i\frac{\partial\psi}{\partial R} + k_{T0}(R)\psi + (M/k_{T0})\left[\frac{1}{2m}\frac{d^2}{dx^2} + \frac{1}{2}V''(R;x_T)x^2\right]\psi = 0 \tag{D2}$$

is then solved exactly by substituting a wave function of the form

$$\psi(R,x) = F(R)\exp\left[iS(R)x^2\right], \tag{D3}$$

and then solving the resulting ordinary differential equations for $F(R)$ and $S(R)$. The trial wave function has the same form as the adiabatic solution along the path in the complex plane that we use. If the adiabatic solution is replaced by the more general form Eq. (D3) as in the theory of Refs. [7] and [3], then the correct Wannier law is obtained. Here we shall use Eq. (D3) to examine a first diabatic correction to the adiabatic solution. To that end we set

$$\begin{aligned}\varphi_{\rm ad1} &= \varphi_T(x)\exp[if(R)x^2] \\ &= \exp\left[i\left(\frac{1}{2}\sqrt{-V''(R;x_T)m} + f(R)\right)x^2\right],\end{aligned} \tag{D4}$$

where $f(R)$ is a small correction to be deduced. This wave function is substituted into the Schrödinger equation

$$i\frac{k_{T0}(R)}{M}\frac{\partial\varphi_{\rm ad1}}{\partial R} - \left[\frac{-1}{2m}\frac{d^2}{dx^2} + \frac{1}{2}V''(R;x_T)\right]\varphi_{\rm ad1} = -[\epsilon_T^{(1)}(R) - V(R;x_T)]\varphi_{\rm ad1}, \tag{D5}$$

and terms of order $f(R)^2$ are dropped. This gives the differential equation for f

$$\frac{\partial f}{\partial R} + \frac{1}{2}\frac{\partial\sqrt{-mV''(R;x_T)}}{\partial R} + \frac{2M}{k_{T0}(R)}\sqrt{\frac{-V''(R;x_T)}{m}}f = 0 \tag{D6}$$

and the first-order eigenvalue

$$\epsilon_T^{(1)}(R) = \epsilon_T(R) - i\frac{f(R)}{m}. \tag{D7}$$

The differential equation (D6) for $f(R)$ is readily solved by standard techniques to give

$$\begin{aligned}f(R) = \frac{1}{2}&\exp\left[-2\int\frac{M}{k_{T0}(R)}\sqrt{\frac{-V''(R;x_T)}{m}}dR\right] \\ &\times\int\exp\left[2\int\frac{M}{k_{T0}(R)}\sqrt{\frac{-V''(R;x_T)}{m}}dR\right] \\ &\times\frac{\partial}{\partial R}\sqrt{\frac{-V''(R;x_T)}{m}}dR\,.\end{aligned} \tag{D8}$$

Note that $f(R)$ and $\epsilon^{(1)}(R)$ depend upon the energy E, as is appropriate for a diabatic energy eigenvalue. Since we are interested in the limit as $E \to 0$, we will evaluate $f(R)$ for $E = 0$. Recalling the value of $k_{T0}(R)$ from Eq. (3.38) and the definition of $\zeta_{\rm ad}$, we have

$$\begin{aligned}f(R) &= -\frac{1}{2}\sqrt{\frac{-V''(R)m}{R}}\exp\left[-2\zeta_{\rm ad}\int R^{-1}dR\right] \\ &\quad\times\int\exp\left[-2\zeta_{\rm ad}\int R^{-1}dR\right]\frac{\partial R^{1/2}}{\partial R}dR \\ &= -\frac{1}{4}\sqrt{\frac{-V''(R)m}{R}}R^{-2\zeta_{\rm ad}}\int R^{2\zeta_{\rm ad}-1/2}dR \\ &= -\frac{1}{8}\sqrt{-\frac{V''(R;x_T)m}{R}}\frac{R^{1/2}}{\zeta_{\rm ad}+1/4}\,.\end{aligned} \tag{D9}$$

This then gives, for the correction term in Eq. (D7), the result

$$-i\frac{f(R)}{m} = -\frac{1}{4}\frac{1}{\zeta_{\rm ad}+1/4}\left(-\frac{i}{2}\sqrt{-\frac{V''(R)}{m}}\right), \tag{D10}$$

where we have used the fact that $V''(R;x_T)m/R$ is independent of R.

Notice that this correction to $\epsilon_T(R)$ equals the imaginary part of the adiabatic eigenvalue $\epsilon_T(R)$ aside from the multiplicative constant $-1/(4\zeta_{\rm ad}+1)$, thus,

$$\zeta^{(1)} = \zeta_{\rm ad}\left(1 - \frac{1}{4\zeta_{\rm ad}+1}\right). \tag{D11}$$

APPENDIX E: ANHARMONIC CORRECTIONS TO WANNIER'S THRESHOLD LAW

In the harmonic-oscillator region we expand the adiabatic eigenvalues $\epsilon_T(R) = \epsilon(R)$ of Sec. III A for $H_2{}^+$ in powers of $R^{-1/2}$;

$$\epsilon_T(R) = -\frac{C_0}{R} - \left(\frac{C_1' + i\sqrt{C_1}/2}{R^{3/2}} + \frac{C_2' + iC_2}{R^2} + \frac{C_3' + iC_3}{R^{5/2}}\right)\left(\frac{1+2\delta_A}{\sqrt{m_0}}\right), \tag{E1}$$

where C_0 and C_1 are given by Eqs. (4.5). For $H_2{}^+$ the constants are

$$C_0 = 3\,; \quad C_1 = 32\,; \quad C_1' = -4\,; C_2 = -3\sqrt{2}\,;$$
$$C_2' = 3/2\,; \quad C_3 = 39\sqrt{2}/16\,; \quad C_3' = 9/16\,. \tag{E2}$$

In this case the probability $P_\infty(E)$ is given by

$$P_\infty(E) = \exp[Q(E)]\,, \tag{E3}$$

where

$$Q(E) = \sqrt{2M}\,\mathrm{Im}\int_{R_0}^{\infty} \frac{\epsilon_T(R) - V(R;x_T)}{\sqrt{E - V(R;x_T)}}\,dR\,. \tag{E4}$$

Substituting Eq. (E1) into Eq. (E4) and doing the integration with the omission of the exponentially small term δ_A, we obtain

$$Q(E) = 2\sqrt{\frac{2M}{m_0 C_0}}\left[\frac{1}{2}\left(\frac{\sqrt{C_1}}{2} - \frac{C_3}{2C_0}E\right)\ln E + \frac{C_2}{\sqrt{C_0}}\sqrt{E} - \left(\frac{C_2}{\sqrt{C_0}} + \frac{C_3}{2\sqrt{C_0 R_0}}\right)\sqrt{E + \frac{C_0}{R_0}} - \left(\frac{\sqrt{C_1}}{2} - \frac{C_3}{2C_0}E\right)\ln\left(\sqrt{\frac{C_0}{R_0}} + \sqrt{E + \frac{C_0}{R_0}}\right)\right]. \tag{E5}$$

In the limit $E \ll 1$;

$$Q(E) = 2\sqrt{\frac{2M}{mC_0}}\left[\frac{\sqrt{C_1}}{4}\ln E + \frac{C_2}{\sqrt{C_0}}\sqrt{E} - \frac{C_3}{4C_0}E\ln E - \left(\frac{\sqrt{C_1}}{4}\ln\frac{4C_0}{R_0} + \frac{C_2}{\sqrt{R_0}} + \frac{C_3}{2R_0}\right) + E\left(\frac{C_3}{4C_0}\ln\frac{4C_0}{R_0} - \frac{C_3}{4C_0} - \frac{C_2}{2C_0}\sqrt{R_0} - \frac{\sqrt{C_1}}{8C_0}R_0\right)\right]. \tag{E6}$$

When $E > 1$ the approximate result is given by

$$Q(E) = -\frac{4}{v}\left(\frac{\sqrt{C_1}}{2\sqrt{R_0}} + \frac{C_2}{2R_0} + \frac{C_3}{3R_0^{3/2}}\right). \tag{E7}$$

For $H_2{}^+$, Eqs. (E6) and (E7) when $R_0 = 4$ give

$$Q(E) = 4\sqrt{\frac{M}{3m}}\left[\ln E - \sqrt{3E} - \frac{13}{64}E\ln E + \left(\frac{153}{128} - \ln 3\right) + E\left(\frac{25}{192} + \frac{13}{64}\ln 3\right)\right] \tag{E8}$$

and

$$Q(E) = -\frac{93\sqrt{2}}{32v}\,, \tag{E9}$$

respectively.

These expressions for $Q(E)$ are approximate since we have omitted the diabatic corrections to C_1'. When these are included, a more accurate approximate expression for $Q(E)$ is given by

$$Q(E) = \zeta\left[\left(1 - \frac{39}{64}\frac{y_0}{R_0}\right)\ln\left(\frac{\sqrt{y_0+1}-1}{\sqrt{y_0+1}+1}\right) - \frac{3}{\sqrt{R_0}}\sqrt{y_0} + \left(\frac{3}{\sqrt{R_0}} - \frac{39}{32}\frac{1}{R_0}\right)\sqrt{y_0+1}\right], \tag{E10}$$

where ζ is Feagin's Wannier index Eq. (4.13) for $H_2{}^+$ and $y_0 = ER_0/C_0$.

[1] G. H. Wannier, Phys. Rev. **90**, 817 (1953).
[2] A. R. P. Rau, Phys. Rev. A **4**, 207 (1971).
[3] R. Peterkop, J. Phys. B **4**, 513 (1971).
[4] H. Klar and W. Schlecht, J. Phys. B **9**, 1699 (1976).
[5] U. Fano, Phys. Today **1**, 1 (1976).
[6] U. Fano, Rep. Prog. Phys. **46**, 97 (1983).
[7] James M. Feagin, J. Phys. B **17**, 2433 (1984).
[8] T. G. Winter and C. D. Lin, Phys. Rev. A **29**, 3071 (1984).
[9] R. E. Olson, Phys. Rev. A **33**, 4397 (1986).
[10] S. Y. Ovchinnikov and E. A. Solov'ev, Zh. Eksp. Teor. Fiz. **90**, 921 (1986) [Sov. Phys. JETP **63**, 538 (1986)].
[11] D. I. Abramov, S. Y. Ovchinnikov, and E. A. Solov'ev, Pis'ma Zh. Eksp. Teor. Fiz. **47**, 424 (1988) [JETP Lett., **47**, 504 (1988)].
[12] S. Y. Ovchinnikov and E. A. Solov'ev, Comments At. Mol. Phys. **XXII**, 69 (1988).
[13] E. A. Solov'ev, Usp. Fiz. Nauk. **157**, 437 (1989) [Sov. Phys. Usp. **32**, 228 (1989)].
[14] D. Jakubassa-Amundsen and J. Macek, J. Phys. A **22**, 4151 (1989).
[15] J. M. Rost, J. S. Briggs, and P. T. Greenland, J. Phys. B **22**, L353 (1989).
[16] J. H. Macek, Phys. Rev. A **41**, 1361 (1990).
[17] E. A. Solov'ev, Phys. Rev. A **42**, 1331 (1990).
[18] S. Yu. Ovchinnikov, Phys. Rev. A **42**, 3865 (1990).
[19] M. Pieksma and S. Y. Ovchinnikov, J. Phys. B **24**, 2699 (1991).
[20] A. K. Kazansky and V. N. Ostrovsky, J. Phys. B **25**, 2121 (1992).
[21] E. A. Solov'ev and S. I. Vinitsky, J. Phys. B **18**, L557 (1985).

[22] J. H. Macek, in *Fundamental Processes of Atomic Dynamics, NATO Advanced Study Institute Series*, edited by J. S. Briggs, H. Kleinpoppen, and H. O. Lutz (Plenum, New York, 1988), pp. 129–142.

[23] L. D. Landau and E. M. Lifshitz, *Quantum Mechanics: Non-Relativistic Theory*, 2nd ed. (Pergamon Press, Oxford, England, 1965).

[24] Yu. N. Demkov, in *Proceedings of Invited Talks of the Fifth International Conference on the Physics of Electronic and Atomic Collisions, Leningrad, 1967*, edited by I. P. Flaks and E. S. Solovyev (Joint Institute for Laboratory Astrophysics, Boulder, CO, 1968), p. 186.

[25] J. H. Macek, J. Phys. B **1**, 1 (1968).

[26] V. Komarov, L. I. Ponamarev, and S. Yu. Slovyanov, *Spheroidal and Coulomb Spheroidal Functions* (Nauka, Moscow, 1976).

[27] *Handbook of Mathematical Functions*, Natl. Bur. Stand. Appl. Math. Ser. No. 55, edited by Milton Abramowitz and Irene A. Stegun (U.S. GPO, Washington, DC, 1965).

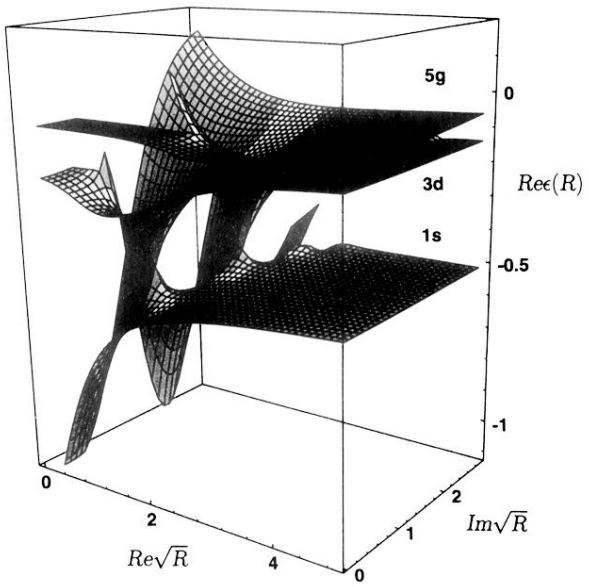

FIG. 1. Plot of the real part of the energy function $\epsilon(R)$ vs complex R. The plot represents a Riemann surface on which $\epsilon(R)$ is a single-valued function. The values along the real axis are the energy eigenvalues $\epsilon_n(R)$ of $H_2{}^+$.

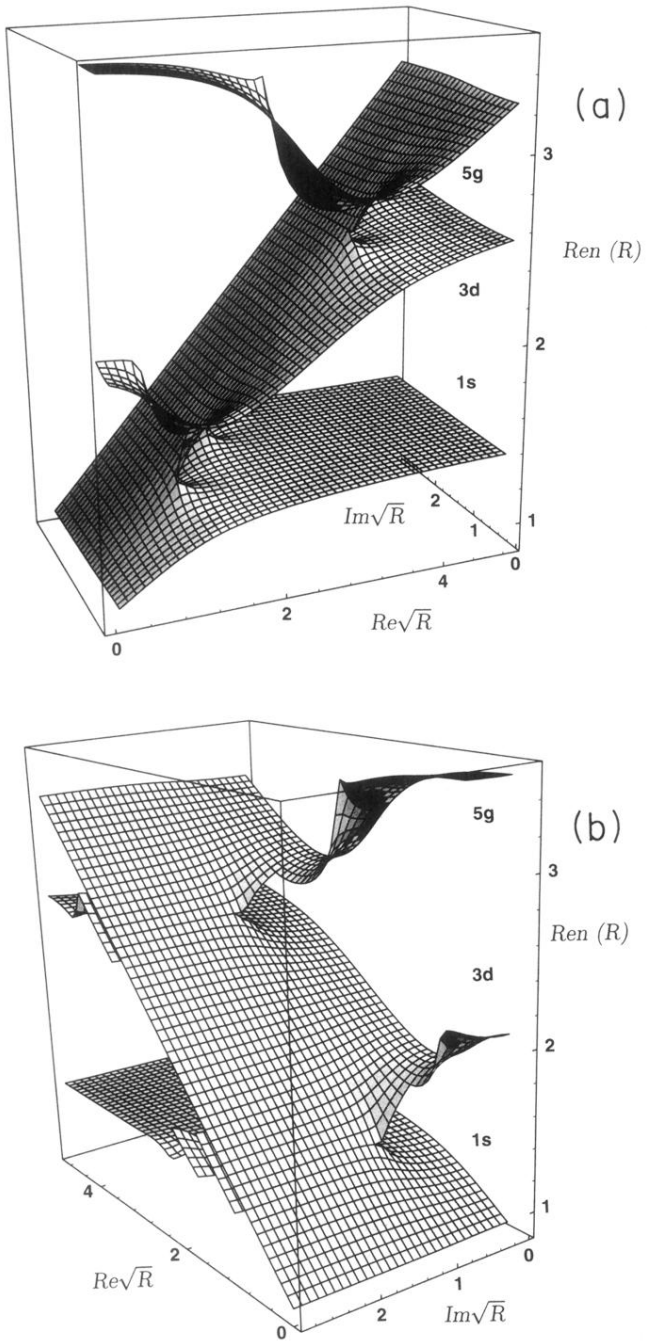

FIG. 2. Plot of $1/\sqrt{\epsilon(R)}$ vs $\sqrt{R}$. (a) "Front" view of the surface with the real axis foremost. (b) "Back" view of the surface showing a sloping flat region to the left of an infinite series of branch points. The first two branch points of this series where the $1s\sigma$-$3d\sigma$-$5g\sigma$ sheets join are exposed in the latter view.